ATLAS–BASED APPROACH FOR THE SEGMENTATION OF INFANT DTI MR BRAIN IMAGES

Mahmoud Mostapha[1]*, Amir Alansary*[1]*, Ahmed Soliman*[1]*, Fahmi Khalifa*[1]*, Matthew Nitzken*[1]*,*
Rasha Khodeir[1]*, Manuel F. Casanova*[2] *and Ayman El-Baz*[1]
[1]BioImaging Laboratory, Bioengineering Department, University of Louisville, Louisville, KY, USA.
[2]Department of Psychiatry and Behavioral Science, University of Louisville, Louisville, KY, USA.

ABSTRACT

In this paper, we propose a new adaptive atlas-based technique for the automated segmentation of brain tissues (white matter and grey matter) from infant diffusion tensor images (DTI). Brain images and desired region maps (brain, Cerebrospinal fluid, etc.) are modeled by a joint Markov-Gibbs random field (MGRF) model of independent image signals and interdependent region labels. The proposed joint MGRF model accounts for the following three descriptors: (*i*) a 1^{st}-order visual appearance to describe the empirical distribution of six features that has been estimated from the DTI in addition to the non-diffusion (b0) scans, (*ii*) 3D probabilistic atlases, and (*iii*) a 3D spatially invariant 2^{nd}-order homogeneity descriptor. The 1^{st}-order visual appearance descriptor, assuming each of the estimated DTI parameters are independent, is precisely approximated using our previously developed linear combination of discrete Gaussians (LCDG) intensity model that includes positive and negative Gaussian components. The 3D probabilistic atlases are learned using a subset of the 3D co-aligned training DTI brain images. The 2^{nd}-order homogeneity descriptor is modeled by a 2^{nd}-order translation and rotation invariant MGRF of region labels, with analytically estimated potentials. We tested our approach on 25 DTI brain images, and evaluated the performance on 5 manually segmented 3D DTI brain images to confirm the high accuracy of the proposed approach, as evidenced by the Dice similarity, Hausdorff distance, and absolute volume difference metrics.

Index Terms— Infant, MGRF, LCDG, DTI Brain Segmentation

1. INTRODUCTION

Diffusion tensor imaging (DTI) is a fairly new MRI modality which was introduced in the mid-1990s [1]. DTI is a noninvasive method that offers valuable information about the structure of the human brain that could not be acquired from conventional MRI. DTI can distinguish water diffusion behavior in brain tissues, such as anisotropic diffusion in white matter. These anisotropic properties are sensitive to the fiber orientation, and can be exploited to define the axonal organization of the brain. DTI is used in a wide range of applications including fiber tracking, a key tool in assessing brain connectivity [2]. Segmentation of different structures (e.g. white matter) is a crucial step in any computer-aided diagnostic (CAD) system for the brain. Although manual segmentation performed by experts remains the gold standard, automatic segmentation approaches are vital due to the time consuming nature and performance variability of manual segmentation procedures.

Accurate segmentation of the grey matter (GM), white matter (WM), and cerebrospinal fluid (CSF) from the whole-brain is an important step used in many fields, such as clinical applications, human brain mapping, and neuroscience. General MRI segmentation methods face multiple challenges that includes image inhomogeneities, image artifacts, such as partial volume effect, and discontinuities of boundaries due to similar visual appearances of adjacent brain structures. In addition, the existence of the diffusion-sensitizing gradient found in diffusion weighted imaging (DWI) produces an amplification effect to the distortions that are linked with patient motion [3]. Moreover, the difficulties in imaging infants' brains, which will be the case study in this paper, are more challenging and stem from the immaturity of the brain tissues, eddy current artifacts, and bulk motion distortions, especially in unseated infants.

Various brain DTI segmentation methods have been employed in the past few years. They can be classified into three main three categories: probabilistic and statistical-based [4, 5], deformable model-based [6, 7], and atlas-based techniques [8, 9]. Due to the space limitations, we will briefly overview some atlas-based methods related to the focus of this paper. For more details please see [10].

Atlas-based segmentation approaches treat the segmentation problem as a registration task, and utilize prior knowledge about brain structures to overcome signal inhomogeneity and overlaps between signal distributions of different brain structures. MRI atlases are often used in studies that focus on grey matter structures while DTI atlases are superior in providing unique information about white matter structures. However, adult-based atlases can't be used to segment infant brains due to the ongoing WM myelination of infant images [11]. Recently, there have been several studies investigating infants brains with autism using an atlas-based framework for their segmentation approach. Neda et al. [12] proposed a segmentation approach that involves two different registration frameworks using DTI and T2-weighted images. The intra-subject and inter-modality registration was based on a multi-scale approach that employs both affine and B-spline transformations, using the normalized mutual information as a matching metric. Scans taken at different time intervals are linearly mapped to an atlas constructed from a patient at the age of one year. They are subsequently mapped using a nonlinear transformation to a T2-weighted atlas, and tensor images are estimated from the aligned DWI and averaged using the log-Euclidean method to produce a final DTI atlas. In summary, the

978-1-4673-1961-4/14/$31.00 ©2014 IEEE

above brief overview shows the following drawbacks that exist in some DTI-based infant brain segmentation: (*i*) using atlases built from different modalities (e.g. T2-weighted and DTI) will affect the segmentation accuracy due to different contrast levels and inter-slice variability, and (*ii*) using nonlinear registration doesn't preserve the shape information, thus limiting the possibility of performing any shape-based analysis on the segmented data, which could be used to investigate the correlation between WM and GM morphology [13].

To overcome these limitations, we propose an atlas-based approach for the accurate segmentation of brain tissues (WM+GM) from DTI images. The proposed approach depends on a combination of both prior information (atlas) and current appearance features of the DTI (the 1^{st}-order visual appearance and the spatial interaction between brain voxels) [14].

2. THE PROPOSED SEGMENTATION FRAMEWORK

In this paper, we propose an automated approach for the extraction of different brain structures from DTI as follows: (*i*) inhomogeneities are reduced, artifacts detected, and motion and eddy current distortions are corrected, (*ii*) DTI generation and its parameters estimation, (*iii*) estimation of both the 1^{st}- and 2^{nd}-order visual appearance models that are required to calculate the proposed joint Markov-Gibbs random field (MGRF) model, (*iv*) initial segmentation of the DTI data using both 1^{st}-order visual appearance models and our prior atlas model, and (*v*) segmentation refinement by integrating 1^{st}-order visual appearance models, 2^{nd}-order spatial interactions model, and prior atlas model in the proposed joint MGRF model. Details of the joint MGRF model are outlined below.

Let $\mathbf{Q} = \{0, \ldots, Q-1\}$ and $\mathbf{L} = \{1, \ldots, L\}$ denote sets of gray levels q and region labels L, respectively. Let $\mathbf{R}$ denote a 3D arithmetic (x, y, z)-lattice supporting a given grayscale image $\mathbf{g} : \mathbf{R} \rightarrow \mathbf{Q}$ to be segmented and its goal labeled region map $\mathbf{m} : \mathbf{R} \rightarrow \mathbf{L}$. The 3D DTI brain images, $\mathbf{g}$, being co-aligned to the 3D training data, and its map, $\mathbf{m}$, are described with the following joint probability model:$P(\mathbf{g}, \mathbf{m}) = P(\mathbf{g}|\mathbf{m})P(\mathbf{m})$, which combines a 3D 2^{nd}-order MGRF ($P(\mathbf{m})$) of region labels with a prior atlas model and a conditional distribution of the images given the map:$P(\mathbf{g}|\mathbf{m}) = \prod_{(x,y,z)\in\mathbf{R}} p(g_{x,y,z}|m_{x,y,z})$. The map model $P(\mathbf{m}) = P_{\rm sp}(\mathbf{m})P_{\rm h}(\mathbf{m})$ has two parts: (*i*) a atlas prior probability $P_{\rm sp}(\mathbf{m})$, and (*ii*) a 2^{nd}-order MGRF model $P_{\rm h}(\mathbf{m})$ of a spatially homogeneous map $\mathbf{m}$ for the image $\mathbf{g}$.

3D Probabilistic Atlas: In order to reduce variability across subjects and obtain a more accurate segmentation, we employed probabilistic atlases of the expected shapes of the brain labels. A training set of images, collected from different subjects, are co-aligned using a 3D affine transformation with 12 degrees of freedom by maximizing their Mutual Information (MI) [15]. The probabilistic atlases are spatially variant independent random fields of region labels $P_{\rm sp}(\mathbf{m}) = \prod_{(x,y,z)\in{\rm R}} p_{{\rm sp}:x,y,z}(m_{x,y,z})$ for the co-aligned manually segmented data sets, specified by voxel-wise empirical probabilities for each brain label ($p_{{\rm sp}:x,y,z}(l), l \in \{1, \ldots, L\}$).

Our framework exploits probabilistic atlases (built at the learning stage) for three labels: brain tissue (GM+WM), CSF, and other brain structures (excluding the background). For the training phase, we use four manually segmented data sets (non-diffusion (b0) scan) by an expert to create the probabilistic maps for the three labels. In the testing phase, each data to be segmented is registered, using an affine 3D registration, with one of the training sets used to create the prior atlas.

1^{st}-Order Visual Appearance Descriptor: In addition to the learned prior atlas descriptor, our approach accounts for the visual appearance of each brain structure in the b0 scan and six other DTI estimated parameters: the three eignvalues ($\lambda 1$, $\lambda 2$, and $\lambda 3$), fractional anisotropy (FA), relative anisotropy (RA), and Trace maps. These six parameters are calculated from the tensor matrix derived from each DTI data set. The mixed empirical marginal 1D distribution of voxel intensities is separated into three individual components, associated with each label of the mixture. To model the current DTI appearance, the empirical distribution is precisely approximated with a linear combination of discrete Gaussians (LCDG) and automatically separated into distinct LCDG components [16]. This approximation adapts the segmentation to the changing appearance, such as non-linear intensity variations caused by patient weight and data acquisition systems. The LCDG models the empirical distribution of the brain labels more accurately than a conventional mixture of only positive Gaussians. This yields a better initial region map that is formed by the voxel-wise classification of the image gray values. The LCDG model is described in detail in [16–18].

3D Spatial Interaction MGRF Model: In order to perform a more accurate segmentation, spatially homogeneous 3D pairwise interactions between the region labels are additionally incorporated in the model. These interactions are calculated using the popular Potts model (i.e., an MGRF with the nearest 26-neighbors of the voxels), and analytic bi-valued Gibbs potentials, that depend only on whether the nearest pairs of labels are equal or not. Let $f_{\rm eq}(\mathbf{m})$ denote the relative frequency of equal labels in the neighboring voxel pairs $((x, y, z), (x+\xi, y+\eta, z+\zeta)) \in \mathbf{R}^2; (\xi, \eta, \zeta) \in \{(\pm 1, 0, 0), (0, \pm 1, 0), (\pm 1, \pm 1, 0), \pm 1, 0, \pm 1), (0, \pm 1, \pm 1), (\pm 1, \pm 1, \pm 1)\}$. The initial region map results in an approximation with the following analytical maximum likelihood estimates of the potentials [16]: $v_{\rm eq} = -v_{\rm ne} \approx 2f_{\rm eq}(\mathbf{m}) - 1$, which that allow for computing the voxel-wise probabilities $p_{{\rm h}:x,y,z}(m_{x,y,z} = \lambda)$ of each brain label; $l \in \mathbf{L}$.

One of the main advantages of the proposed approach is that in addition to the prior information, our approach depends on two other models (1^{st}- and 2^{nd}-order visual appearance models) that are estimated directly from the input data, making our approach adaptive [14, 16–18]. The proposed step-wise segmentation approach is summarized in Algorithm 1.

3. EXPERIMENTAL RESULTS AND CONCLUSIONS

To assess the robustness and computational performance of our approach, we tested it on 25 data sets, and evaluated the performance on 5 manually segmented ground truth data sets, segmented by an expert. Patient data were obtained from the Infant Brain Imaging Study (IBIS) with participants ranging from 6 to

Algorithm 1: Key Steps for the Proposed Segmentation Approach

1. Reduce DWI data inhomogeneities using a Generalized 3D Gauss-Markov random field (GGMRF) model [19].
2. Detect artifacts, correct motion and eddy current distortions and remove images with large artifacts using DTIprep software [20].
3. Derive DTI from DWI, and estimate its six parameters ($\lambda 1$, $\lambda 2$, $\lambda 3$, FA, RA, and Trace) using 3D Slicer [21].
4. Approximate the marginal intensity distribution $P(\mathbf{g})$ of the b0 scan and the six DTI parameters using the LCDG model with three dominant modes.
5. Form an initial region map $\mathbf{m}$ using the marginal estimated density and prior atlas of each label.
6. Find the Gibbs potentials for the MGRF model from the initial map [16].
7. Improve the region map $\mathbf{m}$ using voxel-wise Bayes classifier after integrating the three descriptors in the proposed joint MGRF model.

9 months of age. Diffusion weighted MRI brain scans were obtained from a 3-T Siemens TIM Trio scanners (Siemens Medical Solutions, Malvern, PA.) using the following parameters: field of view of: 190 mm, number of slices: 75–81, a slice thickness: 2 mm, voxel resolution: $2 \times 2 \times 2$ mm^3, TR: 12,800–13,300 ms, TE: 102 ms, variable b values between 0 and 1,000 s/mm^2, 25 gradient directions, and a scan time of 5-6 minutes.

A step-by-step of the proposed segmentation approach is demonstrated in Fig. 1. The input DTI data (Fig. 1(a)) is first smoothed using the Generalized 3D Gauss-Markov random field (GGMRF) model [19] . Then, the image artifacts are removed and motion and eddy current distortions are corrected using the DTIprep software [20] (Fig. 1 (b)). An initial segmentation is obtained using our prior atlas model and the marginal densities estimated from the b0 scan and the six DTI parameters (Fig. 1 (c)). Finally, the initial segmentation is refined using the proposed three descriptors (1^{st}-order visual appearance models, 3D spatial model, and prior atlas model) to achieve the final segmentation as shown in Fig. 1(d).

In order to evaluate the accuracy of our segmentation approach, we use three performance metrics: (*i*) the Dice similarity coefficient (DSC), (*ii*) 95% modified Hausdorff distance (MHD) metric, and (*iii*) percentage absolute volume difference (AVD) [22]. All metrics were obtained by comparing our automated segmentation to the ground truth. The b0 scans from 9 subjects were manually segmented to provide 5 data sets for segmentation evaluation and 4 data sets for the construction of our multi-atlas. As demonstrated in Table 1, the mean DSC, MHD, and AVD values for our automated segmentation of the whole brain (GM + WM) are 90.72$\pm$1.062%, 14.79$\pm$1.249 mm, and 7.335$\pm$5.472%, respectively. This confirms the high accuracy of the proposed segmentation technique.

In conclusion, our experiments show that the proposed accurate identification of the joint MGRF model demonstrates promising results in segmenting brain tissues (GM + WM) from DTI images. Our present implementation in the C++ programming language on a Dell precession T7500 workstation (3.33Ghz Intel quad-core with 48GB RAM) takes about 37.21 ± 43.01 sec to processing each test subject.

In the future, we will construct an atlas for both WM and GM, in order to further classify the segmented brain into the WM and GM. This will help us to perform a connectivity analysis on the WM fiber tracts, and to correlate our findings with brain shape descriptors (e.g. spherical harmonics) to obtain a quantitative marker that can be used in the study of both control and developmental brain disorders (e.g. autism, dyslexia).

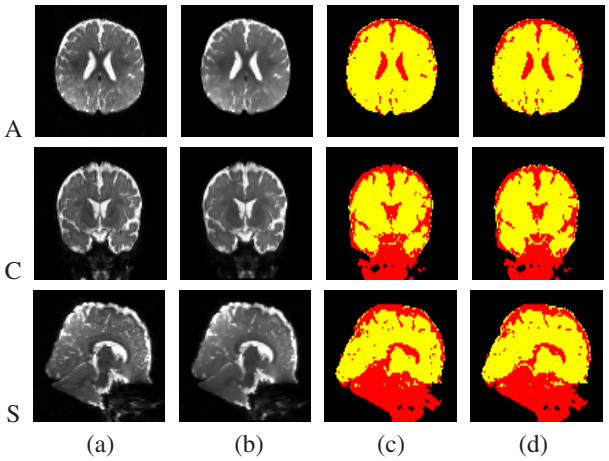

Fig. 1. Segmentation results of the proposed approach. Segmentation is performed in 3D. Results are projected onto 2D axial (A), coronal (C), and sagittal (S) planes for visualization. (a) 2D profile of the original b0 scan images, (b) b0 scan images after MGRF smoothing and preprocessing using DTIprep [20], (c) initial segmentation using 1^{st}-order visual appearance models and prior atlas model, and (d) final segmentation results using the proposed three models. Note that brain tissues (WM+GM) and non-brain tissues are shown in yellow and red, respectively.

Table 1. Accuracy of our segmentation approach using the Dice similarity coefficient (DSC), 95% modified Hausdorff distance (MHD), and percentage absolute volume difference (AVD) for brain tissues (WM+GM) only ("STD– standard deviation").

	Min	Max	Mean	STD
DSC (%)	89.42	91.95	90.72	1.062
MHD (mm)	13.93	17.89	14.79	1.249
AVD (%)	1.991	13.784	7.335	5.472

4. REFERENCES

[1] P. J. Basser, J. Mattiello, and D. LeBihan, "MR diffusion tensor spectroscopy and imaging," *Biophysical Journal*, vol. 66, no. 1, pp. 259–267, 1994.

[2] D. Le Bihan, J.-F. Mangin, C. Poupon, C. A. Clark, S. Pappata, N. Molko, and H. Chabriat, "Diffusion tensor imaging: Concepts and applications," *Journal of Magnetic Resonance Imaging*, vol. 13, no. 4, pp. 534–546, 2001.

[3] T. P. Trouard, Y. Sabharwal, M. I. Altbach, and A. F. Gmitro, "Analysis and comparison of motion-correction techniques in diffusion-weighted imaging," *Journal of Magnetic Resonance Imaging*, vol. 6, no. 6, pp. 925–935, 1996.

[4] S. P. Awate, Z. Hui, and J. C. Gee, "A fuzzy, nonparametric segmentation framework for DTI and MRI analysis: With applications to DTI-tract extraction," *IEEE Transaction on Medical Imaging*, vol. 26, no. 11, pp. 1525–1536, 2007.

[5] Y. Wen, L. He, K. M. von Deneen, and Y. Lu, "Brain tissue classification based on DTI using an improved fuzzy c-means algorithm with spatial constraints," *Magnetic Resonance Imaging*, vol. 31, no. 9, pp. 1623–1630, 2013.

[6] C. Lenglet, M. Rousson, and R. Deriche, "A statistical framework for DTI segmentation," in *Proceedings of IEEE International Symposium on Biomedical Imaging: From Nano to Macro (ISBI'06)*, 2006, pp. 794–797.

[7] L. Jonasson, P. Hagmann, C. Pollo, X. Bresson, C. Richero Wilson, R. Meuli, and J.-P. Thiran, "A level set method for segmentation of the thalamus and its nuclei in DT-MRI," *Signal Processing*, vol. 87, no. 2, pp. 309–321, 2007.

[8] M. Maddah, A. U. Mewes, S. Haker, W. E. L. Grimson, and S. K. Warfield, "Automated atlas-based clustering of white matter fiber tracts from DTMRI," in *Proceedings of International Conference on Medical Image Computing and Computer-Assisted Intervention (MICCAI'05)*, pp. 188–195. 2005.

[9] U. Ziyan, M. R. Sabuncu, W. E. L. Grimson, and C.-F. Westin, "Consistency clustering: a robust algorithm for group-wise registration, segmentation and automatic atlas construction in diffusion MRI," *International Journal of Computer Vision*, vol. 85, no. 3, pp. 279–290, 2009.

[10] A. Elnakib, G. Gimel'farb, J. S. Suri, and A. El-Baz, "Medical image segmentation: A brief survey," in *Multi Modality State-of-the-Art Medical Image Segmentation and Registration Methodologies*, pp. 1–39. 2011.

[11] N. I. Weisenfeld and S. K. Warfield, "Automatic segmentation of newborn brain MRI," *Neuroimage*, vol. 47, no. 2, pp. 564–572, 2009.

[12] N. Sadeghi, M. Prastawa, P. T. Fletcher, J. Wolff, J. H. Gilmore, and G. Gerig, "Regional characterization of longitudinal DT-MRI to study white matter maturation of the early developing brain," *Neuroimage*, 2012.

[13] P. Savadjiev, Y. Rathi, S. Bouix, A. R. Smith, R. T. Schultz, R. Verma, and C.-F. Westin, "Combining surface and fiber geometry: An integrated approach to brain morphology," in *Proceedings of International Conference on Medical Image Computing and Computer-Assisted Intervention (MICCAI'13)*, pp. 50–57. 2013.

[14] A. Alansary, A. Soliman, F. Khalifa, A. Elnakib, M. Mostapha, M. Nitzken, M. Casanova, and A. El-Baz, "Map–based framework for segmentation of mr brain images based on visual appearance and prior shape," *MIDAS Journal [online]. Available: http://hdl.handle.net/10380/3440*, 2013.

[15] P. A. Viola and W. M. W. III, "Alignment by maximization of mutual information," *International Journal on Computer Vision*, vol. 24, no. 2, pp. 137–154, 1997.

[16] A. Farag, A. El-Baz, and G. Gimel'farb, "Precise segmentation of multimodal images," *IEEE Transaction on Image Processsing*, vol. 15, no. 4, pp. 952–968, 2006.

[17] A. El-Baz, *Novel stochastic models for medical image analysis*, Ph.D. thesis, University of Louisville, Louisville, KY, USA, 2006.

[18] A. El-Baz, A. Elnakib, F. Khalifa, M. A. El-Ghar, P. McClure, A. Soliman, and G. Gimel'farb, "Precise segmentation of 3-D magnetic resonance angiography," *IEEE Transaction on Biomedical Engineering*, vol. 59, no. 7, pp. 2019–2029, 2012.

[19] C. Bouman and K. Sauer, "A generalized gaussian image model for edge-preserving MAP estimation," *IEEE Transaction on Image Processsing*, vol. 2, pp. 296–310, 1993.

[20] Z. Liu, Y. Wang, G. Gerig, S. Gouttard, R. Tao, T. Fletcher, and M. Styner, "Quality control of diffusion weighted images," in *Proceedings of SPIE Medical Imaging 2000: Image Processing (SPIE'10)*, 2010, pp. 76280J–76280J.

[21] A. Fedorov, R. Beichel, J. Kalpathy-Cramer, J. Finet, J.-C. Fillion-Robin, S. Pujol, C. Bauer, D. Jennings, F. Fennessy, M. Sonka, et al., "3D slicer as an image computing platform for the quantitative imaging network," *Multidisciplinary Respiratory Medicine*, vol. 30, no. 9, pp. 1323–1341, 2012.

[22] K. O. Babalola, B. Patenaude, P. Aljabar, J. Schnabel, D. Kennedy, W. Crum, S. Smith, T. Cootes, M. Jenkinson, and D. Rueckert, "An evaluation of four automatic methods of segmenting the subcortical structures in the brain," *Neuroimage*, vol. 47, no. 4, pp. 1435–1447, 2009.